International Journal of Pharmaceutics 700 (2026) 127094

Contents lists available at ScienceDirect

International Journal of Pharmaceutics

journal homepage: www.elsevier.com/locate/ijpharm

Functionalized smart surfaces to control the wound healing after glaucoma's surgery

Mónica Machado [a,*], Gabriela Araujo Silva [a], Joana Ferreira [b,c], Luis A. Pinto [b,c], Quirina Ferreira [c,d]

[a] Gene Therapy Lab, iNOVA4Health, NOVA Medical School, Universidade Nova de Lisboa, Campo Mártires da Pátria 130, Lisboa, Portugal
[b] Ophthalmology Department, Santa Maria Local Health Unit, Lisbon 1649-035, Portugal
[c] Visual Sciences Study Centre, Faculty of Medicine, University of Lisbon, Lisbon 1649-028, Portugal
[d] Lisbon School of Health Technology, Polytechnic Institute of Lisbon, Av. Dom João II, Lote 4.6901, 1900-096 Lisbon, Portugal

ARTICLE INFO

Keywords:
Drug-delivery
Encapsulation
Glaucoma
5-Fluorouracil
β-cyclodextrin
Fibroblasts

Chemical compounds studied in this article:
5-Fluorouracil (5-FU)
β-Cyclodextrin (β-CD)
Poly(β-cyclodextrin)
Graphene oxide (GO)
Aminated Graphene Oxide (GO+)
Poly(β-amino ester) (PBAE)
Poly(methyl methacrylate) (PMMA)

ABSTRACT

Over the past decade, considerable attention has been directed toward the development of drug delivery systems capable of releasing therapeutic agents in a controlled and sustained manner over extended periods. Glaucoma, one of the leading causes of irreversible blindness worldwide, is commonly managed with topical eye drops. However, this treatment strategy often suffers from poor patient compliance and limited efficacy. When pharmacological therapy is insufficient, surgical intervention becomes necessary. Among the available surgical options, implantation of drainage devices to divert aqueous humor is widely performed. Despite their functional performance, postoperative wound healing frequently induces an exaggerated fibroblast response that obstructs the drainage channel, resulting in bleb failure. Consequently, the long-term success rate of such procedures is reported to be approximately 70% at one year. To mitigate this challenge, strategies involving localized and time-controlled delivery of antifibrotic drugs have been investigated. In the present study, a nanostructured film was engineered to release precise doses of the antimetabolite 5-Fluorouracil (5-FU) at defined time intervals, aiming to modulate post-operative scarring. Previous work has demonstrated that encapsulation of 5-FU within β-Cyclodextrin (β-CD) cavities enhances drug solubility and reduces toxicity. Building on this concept, films were fabricated on quartz and poly(methyl methacrylate) (PMMA) substrates using the layer-by-layer (LBL) technique.

Film growth and drug release kinetics were successfully monitored by ultraviolet–visible spectroscopy (UV–Vis), demonstrating that PMMA substrates enable a more sustained and prolonged drug release compared to quartz. In conclusion, these findings highlight the significant advantages of polymeric materials commonly used in biomedical devices and wound-contact applications for controlled drug delivery systems.

1. Introduction

Glaucoma represents a major global public health challenge and is widely recognized as one of the leading causes of irreversible blindness worldwide. Epidemiological data consistently highlights both its high prevalence and its growing burden, driven largely by population ageing and increased life expectancy. Globally, it is estimated that glaucoma affected approximately 76 million individuals in 2020, with projections suggesting an increase to 111.8 million by 2040 (Júnior et al., 2025). In terms of visual impairment, glaucoma remains a leading cause of irreversible blindness. In 2020, approximately 3.61 million people were blind and 4.14 million were visually impaired due to glaucoma, accounting for around 8.4% of global blindness (Vision and Eye Research Institute et al., 2024). Unlike other major causes of vision loss, such as cataracts, glaucoma-induced damage is permanent, which significantly amplifies its long-term societal and clinical impact.

The prevalence of glaucoma varies according to age, ethnicity, and geographic region. Globally, the prevalence of primary open-angle

Abbreviations: EDC, N-ethyl-N'-(3-dimethylaminopropyl)carbodiimide methiodide; IOP, Intra ocular pressure; 5-FU, 5-Fluorouracil; β-CD, β-Cyclodextrin; UV–Vis, Ultra violet-visible spectroscopy; LBL, Layer-by layer assembly; GO^{+}, Positively charged graphene oxide; GO^{-}, Negatively charged graphene oxide; PBAE, Poly (β−amino ester); PBS, Phosphate Buffer Saline solution; PMMA, Poly (methyl methacrylate.

* Corresponding author.
E-mail address: a2021086@nms.unl.pt (M. Machado).

https://doi.org/10.1016/j.ijpharm.2026.127094
Received 17 April 2026; Received in revised form 13 June 2026; Accepted 13 June 2026
Available online 15 June 2026

glaucoma (POAG), the most common subtype, is estimated at approximately 2.2–2.4% in the adult population, increasing substantially with age (Allison et al., 2020; Zhang et al., 2021). In individuals over 75 years of age, prevalence can reach up to 10%, highlighting ageing as the most significant risk factor (Allison et al., 2020). Regional disparities are also evident, with higher prevalence and disease burden observed in populations of African descendent and in Sub-Saharan Africa (Vision and Eye Research Institute et al., 2024). Importantly, glaucoma is often asymptomatic in its early stages, and it is estimated that over 50% of cases remain undiagnosed, contributing to delayed treatment and increased risk of irreversible vision loss.

From a longitudinal perspective, the global burden of glaucoma has increased markedly over recent decades. Data from the Global Burden of Disease study indicates an 86% increase in the number of prevalent cases between 1990 and 2021, alongside a substantial rise in disability-adjusted life years (DALYs) associated with the disease (Peng et al., 2026). This trend reflects both demographic changes and persistent challenges in early detection and management.

Glaucoma constitutes a significant and expanding global health problem, characterized by high prevalence, strong age dependence, and marked geographic and ethnic disparities. It is primarily characterized by elevated intraocular pressure (IOP) resulting from obstruction of aqueous humor drainage pathways. Current treatments focus on lowering and controlling IOP, most often through the daily administration of topical eye drops. These drops reduce IOP either by suppressing aqueous humor production or by enhancing its outflow. However, patient adherence to these regimens is frequently poor, often resulting in inadequately controlled IOP (Luís Occhiuto et al., 2019; Rahic et al., 2021). When pharmacological therapy fails, surgical intervention becomes necessary. Procedures such as trabeculectomy or implantation of glaucoma drainage devices (tube shunts) are commonly performed to create an alternative pathway for aqueous humor outflow (Rahic et al., 2021). Although initially effective, the long-term success rates of these procedures are limited, approximately 70–80% in the first year, declining to nearly 50% by the fifth year. This reduction is largely attributed to postoperative wound healing, during which excessive fibroblast proliferation obstructs the drainage channel created by the implant (Schoenberg et al., 2015). Fibroblasts play a central role in the proliferative phase of wound healing, and their growth can be inhibited with antimitotic agents such as 5-FU and Mitomycin C. While widely recognized as chemotherapeutic drugs, these compounds also exhibit potent antiproliferative properties. Specifically, 5-FU acts during the S phase of the cell cycle, inhibiting DNA synthesis and ultimately leading to cell death (Rahic et al., 2021).

Several strategies have been explored to suppress fibroblast proliferation, including intraoperative application of 5-FU for a few minutes or postoperative subconjunctival injections administered over several days (EV Guimarães et al., 2019; Jampel and Henry, 1992; Kristina Reinthal et al., 2007; Svetozarskiy et al., 2023). However, these approaches require relatively high doses to achieve efficacy, and even minimal concentrations may cause significant side effects such as corneal epitheliopathy and erosion (Svetozarskiy et al., 2023). The combination of toxicity, transient effectiveness, and patient discomfort underscores the urgent need for novel drug delivery systems capable of releasing controlled amounts of antifibrotic drugs throughout the wound healing period. Such systems could minimize tissue irritation, improve drug solubility, enhance targeting, and increase bioavailability (Luís Occhiuto et al., 2019).

To address these challenges, the present study investigates the development of a nanostructured drug delivery film with time-controlled release properties. The system consists of alternating drug delivery and barrier layers: the delivery layers incorporate 5-FU encapsulated in β-CD to improve solubility and reduce toxicity, while the barrier layers are composed of a water-soluble poly(β-amino ester) (PBAE) and graphene oxide. Previous studies have demonstrated that the incorporation of PBAE and graphene oxide into LBL assembled films enables fine modulation of drug release profiles. Notably, the addition of a single bilayer of graphene oxide has been shown to delay drug release for more than 24 h while maintaining excellent biocompatibility, underscoring the potential of this architecture for ocular applications (Machado et al., 2019).

In the development of these multilayered films, two different substrates were employed: quartz and PMMA. Quartz substrates offer a smooth, inert, and optically transparent surface, making them particularly suitable for spectroscopic monitoring of film growth and drug release kinetics. However, PMMA is a widely used polymer in ophthalmic devices, intraocular lenses and contact lenses due to its excellent biocompatibility, optical clarity, and mechanical stability (Boyd et al., 1998; Riaz et al., 2014). Clinical studies have shown that rigid PMMA intraocular lenses achieve visual outcomes comparable to foldable lens materials, with more than 90% of patients reaching a visual acuity of 6/18 or better after implantation (Riaz et al., 2014). In addition, PMMA demonstrates high light transmittance in the visible spectrum and minimal cytotoxicity when properly processed, reinforcing its suitability for ocular drug delivery systems (Ferreira et al., 2019; Choi et al., 2014). Its mechanical flexibility and long-term biostability provide further advantages for integration into implantable ophthalmic devices, making it a more clinically relevant substrate compared to quartz.

By enabling sustained and localized delivery of 5-FU, this approach has the potential to overcome the limitations associated with conventional antifibrotic administration, thereby improving the success rate and long-term outcomes of glaucoma drainage surgeries.

2. Material and methods

2.1. Materials

2.1.1. β-CD polymer

β-CD polymer (Lot.BCBP2438V), 5-FU (CAS: 51-21-8, Lot. MK3Q5586V), Phosphate Buffer Saline (PBS) aqueous solution, and PMMA were purchased from Sigma-Aldrich.

2.1.2. Synthesis of β-CD:5-FU complex

The encapsulation of 5-FU in β-CD polymer cavity was made according to the literature (Machado et al., 2025) at the same conditions with a pH 7,1 due to the pH of the Poly(β-amino-ester) polymer (PBAE) solubility.

2.1.3. Synthesis of PBAE

The synthesis of PBAE was made following the protocol described by Lynn *et al.* (Lynn et al., 2020). 3.28 g of 4,4′-trimethylenedipiperidine (97% purity, Sigma Aldrich) and 2.87 ml of 1,4-butanediol diacrylate (99% purity, Alfa Aesar) were mixed in dry tetrahydrofuran (THF) (previously distilled). The copolymerization was carried out under 50°C for 48 h. The final product was purified through repeated precipitations into diethyl ether. PBAE was dried under vacuum overnight.

2.1.4. Positively charged graphene oxide (GO^+)

GO^+ was synthesized following the method developed by Hwang et al. (Hwang et al., 2012). 50 ml of GO^- solution were mixed with 0.625 g of N-ethyl-N'-(3-dimethylaminopropyl)carbodiimide methiodide (EDC) (Sigma Aldrich) and with 5 ml of ethylenediamine (Sigma Aldrich) at room temperature for 24 h.

2.1.5. Negatively charged graphene oxide (GO^-)

GO^- was purchased from Graphenea, as an aqueous dispersion of nanosheets with a concentration of 0.05 mg/ml.

2.2. Methods

2.2.1. Preparation of the substrates

Two different substrates were employed for the fabrication of the multilayered drug delivery films: quartz and PMMA.

Quartz substrates. Rectangular quartz slides (12 × 40 mm, UQG OPTICS) were selected owing to their high optical transparency and chemical inertness, which make them particularly suitable for spectroscopic monitoring of film growth and drug release kinetics. Prior to use, the substrates were subjected to a rigorous cleaning procedure to remove organic and inorganic contaminants. Briefly, slides were immersed in freshly prepared piranha solution, a well-established oxidative treatment that effectively eliminates residual organic material and generates a highly hydrophilic surface. After treatment, the slides were rinsed extensively with tap water, followed by sequential washes with distilled water and HPLC-grade propan-2-ol to ensure removal of residual acid and surface impurities. The cleaned substrates were subsequently dried under a stream of high-purity nitrogen gas to prevent particle deposition from the ambient environment.

PMMA substrates. PMMA substrates were fabricated in-house to provide clinically relevant support for ocular applications, given the widespread use of PMMA in intraocular lenses and its favorable biocompatibility and optical properties. A total of 2gr of PMMA powder was dissolved in 10 ml of chloroform under ambient conditions to obtain a homogenous polymer solution. The mixture was deposited onto a pre-cleaned glass mold using a drop-casting technique and allowed to dry at room temperature. After solvent evaporation, the solidified PMMA film was carefully detached from the mold and transferred to an ethanol bath, where it was subjected to ultrasonic cleaning for 5 min to remove residual solvent traces and surface contaminants (Kaliramna et al., 2022; Wei et al., 2011; Shi et al., 2019). The substrate was sterilized under ultraviolet irradiation for 5 min and the result can be seen in Fig. 1.

2.2.2. Ultraviolet–visible spectroscopy (UV–Vis)

A Jasco V-730 spectrophotometer was used to monitor the growth of the nanostructured films, the drug release kinetics, and the quantification of 5-FU adsorbed within the LBL films.

A calibration curve for 5-FU was established using standard solutions prepared in phosphate-buffered saline (PBS) at concentrations of 0.05, 0.5, 1, 5, 10, 15, 20 and 25 μg/ml. All standards were analyzed under the same experimental conditions employed for sample measurements, enabling the correlation between absorbance and 5-FU concentration to be determined according to the Beer-Lambert law. Linear regression analysis of the calibration data yielded a coefficient of determination (R^2) of 0.99724, demonstrating excellent linearity within the studied concentration range. The limit of detection (LOD) and limit of quantification (LOQ), calculated according to ICH guidelines, were determined to be 1.66 μg/ml and 5.04 μg/ml, respectively. The results confirm the high sensitivity and suitability of the analytical method for the quantitative determination of 5-FU.

2.2.3. Film assembly by layer-by-layer (LBL) technique

Multilayered films were prepared on quartz and PMMA substrates using the LBL adsorption method, schematically represented in Fig. 2 (Le Floch et al., 2020). Prior to film deposition, all substrates were pre-treated with UV-oxygen plasma in a vacuum chamber (Plasma Cleaner PDC-002-CE, Harrick Plasma) to increase surface hydrophilicity and improve subsequent polymer adsorption.

The immersion times for each solution were selected based on previously optimized conditions and applied to the present study (Machado et al., 2019).

LBL film deposition was carried out by sequential immersion of the substrates, handled with tweezers, into the corresponding precursor solutions. Film assembly was initiated with the deposition of PBAE for 7 min as the first layer. After each adsorption step, the substrates were rinsed with sodium acetate solution to remove physiosorbed material and dried under a nitrogen stream. Following PBAE deposition, the substrates were immersed in a β-CD:5-FU solution for 6 min, rinsed with sodium acetate solution, and dried under nitrogen flow. These two successive deposition steps constituted one bilayer (PBAE/ β-CD:5-FU). This bilayer assembly was repeated eight times to generate a “pillow layer” composed of eight PBAE/β-CD:5-FU bilayers.

After formation of the pillow layer, film growth and component incorporation were monitored by UV–Vis spectroscopy. The substrates were again immersed in the PBAE solution, rinsed, and dried, followed by exposure to the β-CD:5-FU solution. After washing and drying, an absorption spectrum was recorded to confirm the drug incorporation within the multilayer structure.

Subsequently, GO deposition was performed by sequential immersion of the substrates into GO^+ and GO^- solutions for 5 min each, with intermediate rinsing and nitrogen drying steps. A second UV–Vis absorption spectrum was acquired after this process to confirm successful GO deposition.

This complete deposition cycle-comprising PBAE, β-CD:5-FU, GO^+, and GO^- deposition, was repeated eight times on quartz substrate to obtain films with eight multilayer units, as schematically illustrated in Fig. 3, with UV–Vis monitoring performed after each cycle. For PMMA substrates, the same procedure was applied but limited to four cycles, resulting in films composed of four multilayer units.

2.2.4. In vitro drug release study

The release kinetics of 5-FU from two multilayered films deposited on quartz and PMMA substrates (48 cm^2) were evaluated under

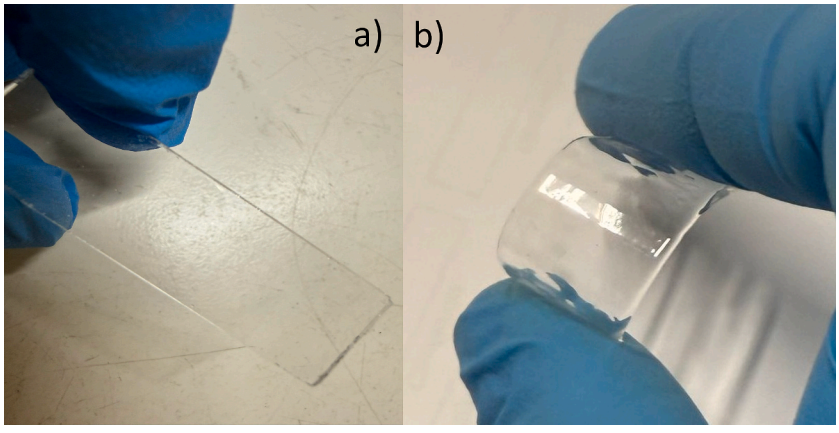

Fig. 1. (a) Quartz substrates and b) PMMA substrates, showing its transparency and PMMA flexibility.

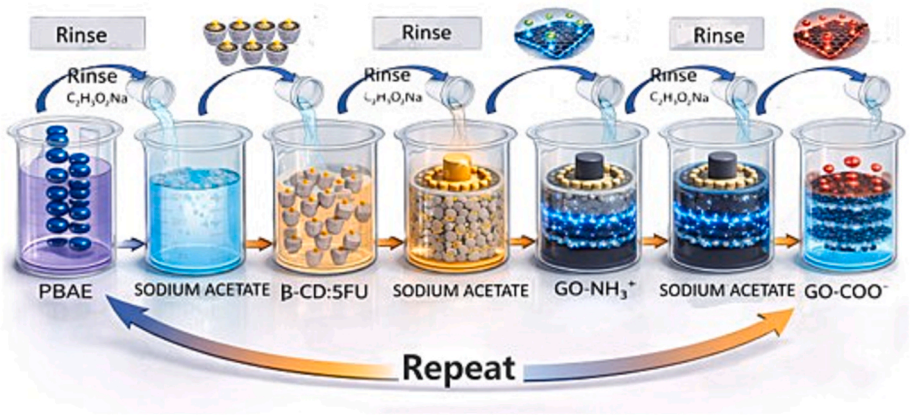

Fig. 2. LBL technique applied to the adsorption of the barrier and drug delivery layers.

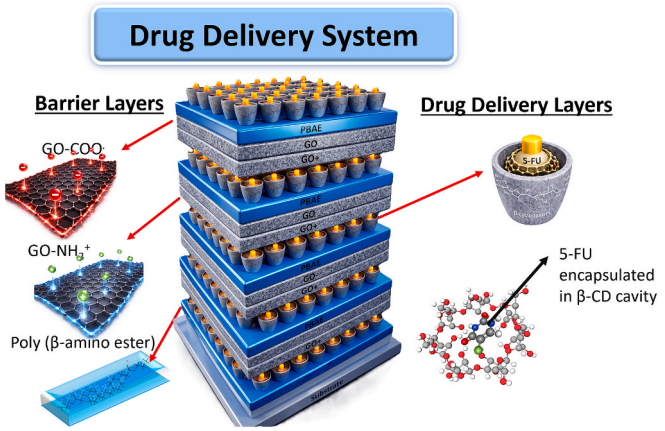

Fig. 3. Schematic representation of the drug delivery system with barrier and drug delivery layers.

simulated physiological conditions. Multiple multilayer films with different numbers of deposition cycles were initially fabricated and characterized to evaluate film growth linearity, structural stability, and reproducibility of the LBL process. The two multilayer configurations presented in this study were subsequently selected for the release assays based on their structural organization and controlled release behavior. The drug-loaded films were immersed in 10 ml of PBS solution at pH 7.4 and maintained at 37°C under gentle agitation to reproduce physiological ionic strength and pH conditions.

At predetermined time intervals, 2 ml of the release medium was withdrawn and transferred into sterile Eppendorf tubes for quantitative analysis. Immediately after each sampling, an equal volume of fresh PBS (2 ml) was added to the release vessel to maintain sink conditions and a constant total volume throughout the experiment. Sampling was performed at short intervals during the initial release phase to capture potential burst release behavior, followed by daily sampling for up to 7 days, and subsequently every 48 h. The release study was conducted for up to 4 days for films deposited on quartz substrates and 56 days for films deposited on PMMA substrates.

UV–Vis absorption spectra were recorded for both the collected PBS aliquots and the remaining films on the substrates at each time point. Quantification of released 5-FU was performed using its characteristic absorption maximum at 265.5 nm, with calibration curves constructed from standard 5-FU solutions prepared in PBS to ensure accurate concentration determination. The cumulative amount of released drug was calculated by summing the amount of 5-FU detected in each collected aliquot, accounting for the replenished volume, and was expressed as μg/ml.

2.2.5. *Atomic force microscopy (AFM)*

Two identical multilayer films were fabricated on quartz substrates, differing only in the composition of the outermost layer, namely graphene or β-CD:5-FU. Surface morphology and nanoscale topography of the films were characterized by AFM operating in non-contact mode.

AFM measurements were performed using a NanoObserver from Concept Scientific Instruments (CSI) equipped with silicon probes (APPPNano). Images were acquired under ambient conditions to minimize sample perturbation. The obtained AFM data, including topography, amplitude and phase images, were processed and analyzed using Gwyddion software.

2.2.6. *Profilometry*

The thikness of the nanostructured film was measured using a Veeco Dektak 6 M profilometer operated in step-height mode with a 3.00 mg applied force. A controlled scratch was introduced into the coated region to expose the underlying substrate, thereby enabling accurate determination of the height discontinuity associated with the multilayer assembly. The resulting topographical profile displayed two-well defined plateaus corresponding to the film surface and the bare substrate, separated by a sharp step characteristic of the LBL coating. After baseline correction and removal of minor surface noise, the height difference between the plateaus was calculated by averaging multiple points within each region.

3. Results and discussion

3.1. *Drug release kinetics*

3.1.1. *Quartz substrate*

The growth of the LBL films deposited on quartz substrates was evaluated in order to confirm the successful sequential assembly of the multilayer architecture. Film buildup was monitored throughout the deposition process by UV–Vis spectroscopy, enabling the assessment of the progressive increase in film thickness and material adsorption after each deposition cycle. The obtained growth profile presented in Fig. 4 provides insight into stability, reproducibility, and organization of the multilayer system, as well as the effectiveness of the electrostatic interactions governing film assembly.

Fig. 4 depicts the progressive increase in intensity of the 16 total bilayers, including 8 PBAE/β −CD:5FU and 8 GO^{+}/GO^{-} bilayers, after UV–Vis absorption.

The 5-FU release kinetics was monitored by UV–Vis of the immersion solutions at each point given by the cumulative concentration of 5-FU along time (Figs. 5 and 6). The cumulative concentration was calculated by the absorbance intensity at the absorbance wavelength of 5-FU (265,5nm) applied to the calibration curve of 5-FU in PBS solution.

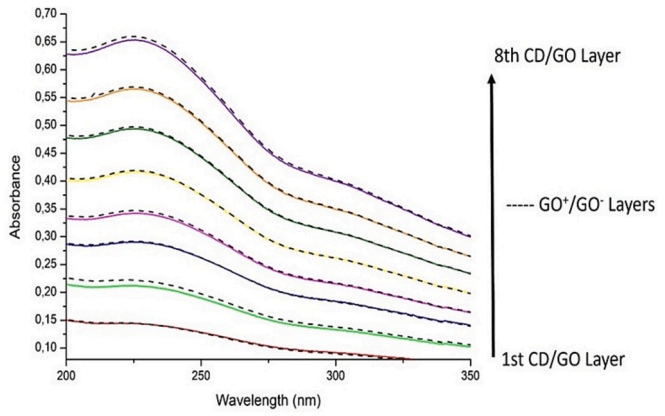

Fig. 4. Absorption spectra of 8 PBAE/β-CD:5-FU bilayers (solid line) and 8 GO^{+}/GO^{-} bilayers (dotted line), showing a progressive increase in intensity, indicating adsorption of each bilayer.

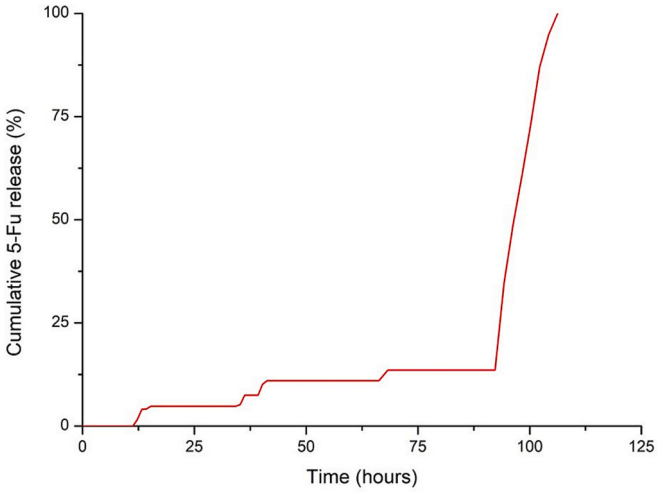

Fig. 5. 5-FU amount released to the PBS solution during the immersion time in a quartz substrate.

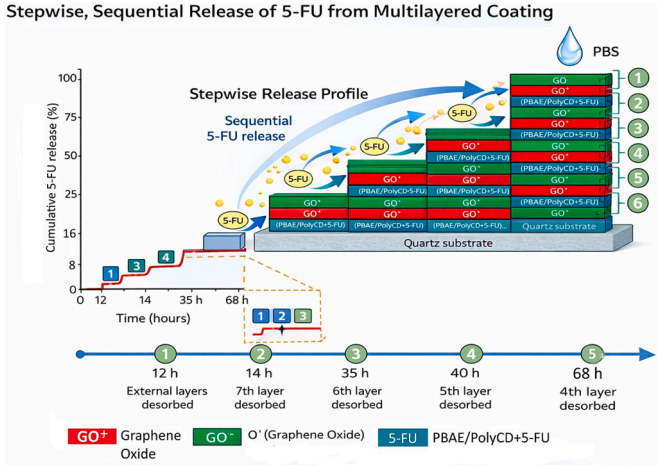

Fig. 6. Representation of 5-FU amount released to the PBS solution during the immersion time compared to the respective drug delivery layer in a quartz substrate.

Fig. 7 shows the cumulative 5-FU release profile from the multilayered (PBAE/ β-CD:5-FU) coating in PBS, together with a schematic representation of the sequential LBL disassembly. The release profile exhibits a characteristic stepwise behavior, where each increase in cumulative release corresponds to the desorption of a specific drug-loaded layer, as illusttrated in the schematic.

The first release event occurs at approximately 12h42min and is attributed to the dedorption of the outermost drug-loaded layers, which are more exposed and weakly bound. This is followed by the release of the 7th layer at approximately 14 h42 min. As the process continues, progressively longer times are required to release the inner layers, with the 6th, 5th 4th, and 3rd layers being released at approximately 35h42min, 40h42min, 68h42min, and 94h42min, respectively. This increasing delay between consecutive release events, clearly supported by both the relase profile and the schematic representation, indicates a progressive increase in intermolecular interactions and atructural stability within the multilayer film. The inner layers are more compact and less accessible to the surrounding medium, requiring longer times for water penetration, polymer swelling, and disruption of host–guest interactions between β-CD and 5-FU. Overall, the results demonstrate a controlled, sequential, and time-resolved drug release mechanism, with the six outermost drug-loaded layers being released over approximately four days. This behavior highlights the potential of the multilayer system for sustained and programmable drug delivery applications.

3.1.2. PMMA substrate

The adsorption of each layer was monitored by UV–Vis spectroscopy, and the film growth profile is presented in Fig. 8. The results demonstrate a sequential and progressive increase in absorbance intensity with each deposition cycle, confirming the orderly and reproducible assembly of the multilayer structure. The linear correlation between absorbance and the number of bilayers is characteristic of the LBL technique and is widely reported in the literature as evidence of uniform film growth and effective adsorption of both drug-delivery and barrier components (Machado et al., 2019). This behavior confirms the robustness of the fabrication process and demonstrates that the incorporation of β-CD:5-FU and barrier materials (PBAE and GO) was achieved in a controlled and reproducible manner, which is essential for ensuring reliable drug release kinetics, as interpolated in Fig. 9.

The adsorption of each layer was monitored by UV–Vis spectroscopy, revealing a sequential and progressive increase in absorbance intensity with each deposition cycle (Fig. 8). This linear correlation between absorbance and the number of bilayers confirms the uniform, reproducible, and well-controlled assembly for the multilayer structure, which is a hallmark of the LBL technique ans consistent with previous studies (Machado et al., 2019).

This behavior demonstrated the successful and predictable incorporation of both drug-delivery layers (β-CD:5-FU) and barrier components (PBAE and GO), ensuring structural integrity and enabling precise control over drug release kinetics.

The release profile obtained for PMMA substrates (Figs. 9, and 10) shows a distinct dual-phase behavior. An initial burst release occurs within the first 24 min, corresponding to the rapid desorption of the outermost drug-loaded layer, which is directly exposed to the surrounding medium. This is followed by a sustained release phase, where progressively longer times are required to the desorption of inner layers. As illustrated in the schematic representation (Fig. 11), the 3rd and 2nd layers are released at approximately 3 h and 12 days, respectively, while deeper layers require significantly longer times, culminating in complete drug release after approximately 56 days. This progressive delay in release is attributed to increasing diffusion resistance, polymer relaxation, and stronger host–guest interactions between β-CD and 5-FU within the inner regions of the multilayer film.

3.2. Surface characterization

Comparative AFM analysis revealed distinct nanoscale differences between β-CD:5-FU and graphene outer layers (Figs. 12 and 13). The

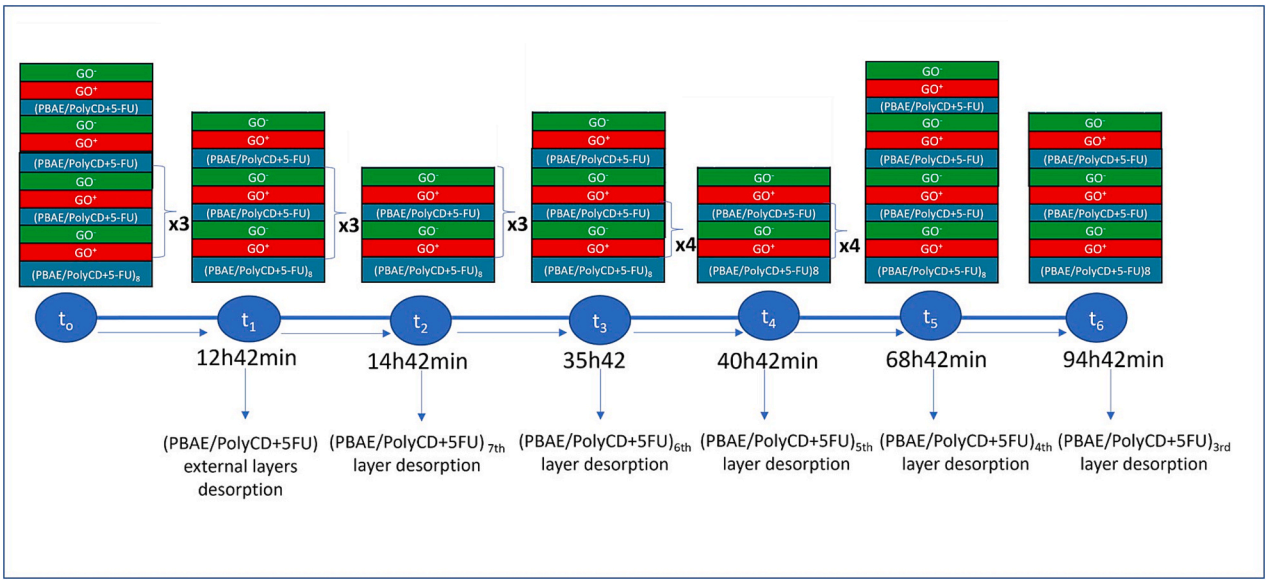

Fig. 7. Diagram of the time release of each drug delivery layer in a quartz substrate. The external drug layer was released after 12 h and 42 min and for the desorption of the 3rd internal layers 4 days were needed.

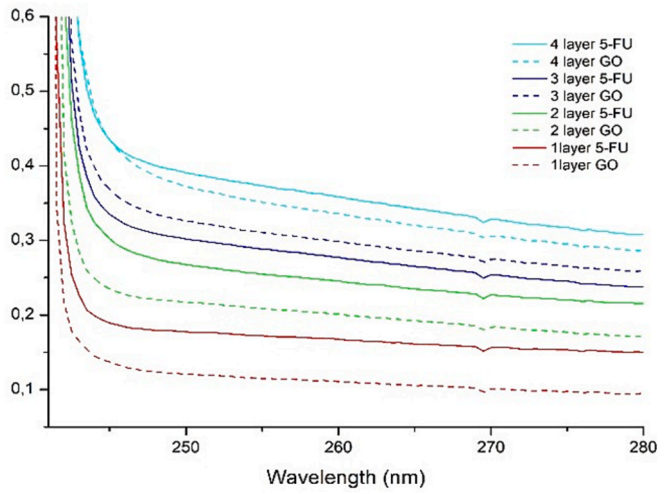

Fig. 8. Absorption spectra of the 4 bilayer PBAE/β-CD (solid line) and bilayer GO^{+}/GO^{-} (dotted line) in a PMMA substrate. It shows a linear increase in intensity with the adsorption of the layers.

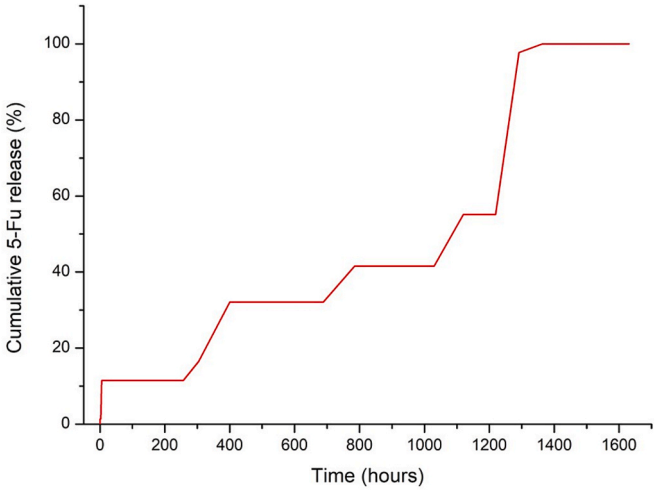

Fig. 9. 5-FU amount release to the PBS solution along the immersion time in a PMMA substrate, represented as interpolation line.

β-CD:5-FU outer layer exhibited a smooth and continuous surface, characterized by limited height variation in the topographical images, uniform amplitude contrast, and gradual phase variations without sharp boundaries (Fig. 12a–c). These festures indicate a mechanically homogeneous and polymer-rich outer layer. Such a uniform nanoscale organization is consitent with enhanced surface hydration and the presence of unobstructed diffusion pathways, which correlate with the experimentally observed sustained release of 5-FU over time (Figs. 10 and 11). This behavior is further supported by the 3D topographical representation (Fig. 14), which suggest the formation of a continuous film composed of irregularly distributed nanoscale domains, likely associated with the molecular organization and aggregation of 5-FU within the LBL architecture. Importantly, the absence of sharp peaks or deep voids indicates uniform film deposition and complete surface coverage, reinforcing the structural integrity of multulayer system and its suitability for controlled drug delivery applications. In contrast, the graphene outer layer showed pronounced platelet-like features, increased surface roughness, strong amplitude contrast, and sharp phase transitions (Fig. 13a–c), indicative of mechanically rigid and heterogeneous graphene domains embedded within multilayer structure. The strong spatial correlation between topography, amplitude, and phase festures in the graphene-containing layer supports the interpretation that rigid graphene domains locally restrict polymer chain mobility and solvent penetration, thereby reducing effective diffusion pathways. Overall, these AFM observations provide a mechanistic basis for understanding differences in drug release behavior between the two layers. While β-CD:5-FU layers are expected to promote sustained and relatively uniform release, graphene layers introduce nanoscale structural and mechanical heterogeneity that can supress or modulate drug releade by limiting diffusion patways. These findings highlight the importance of nanoscale film architecture in controlling drug release kinetics in LBL-based delivery platforms.

3.3. *Film thickness*

The thickness of the nanostructured film was measured using a stylus profilometer. The resulting topographical profile displayed two-well

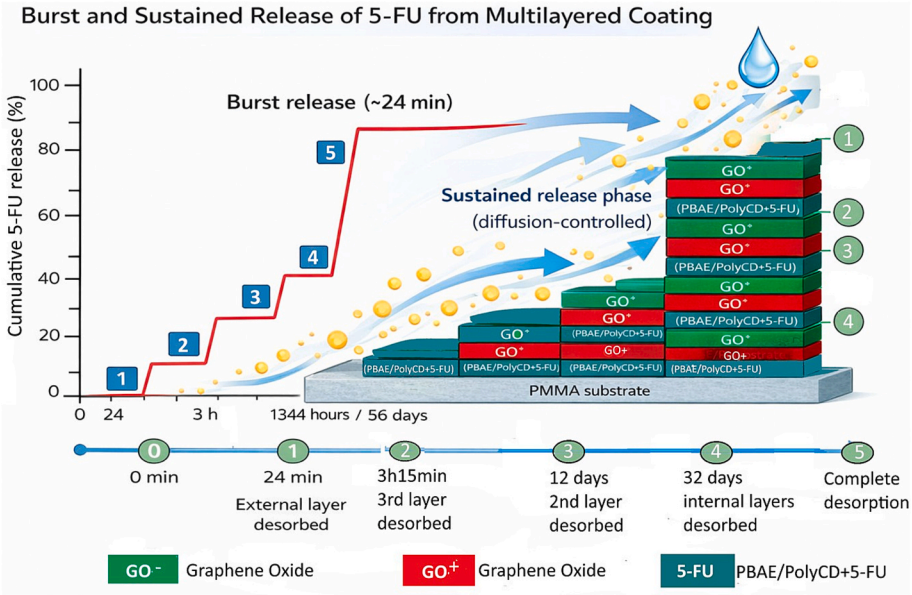

Fig. 10. Representation of 5-FU amount release to the PBS solution along the immersion time compared to the respective drug delivery layer in a PMMA substrate.

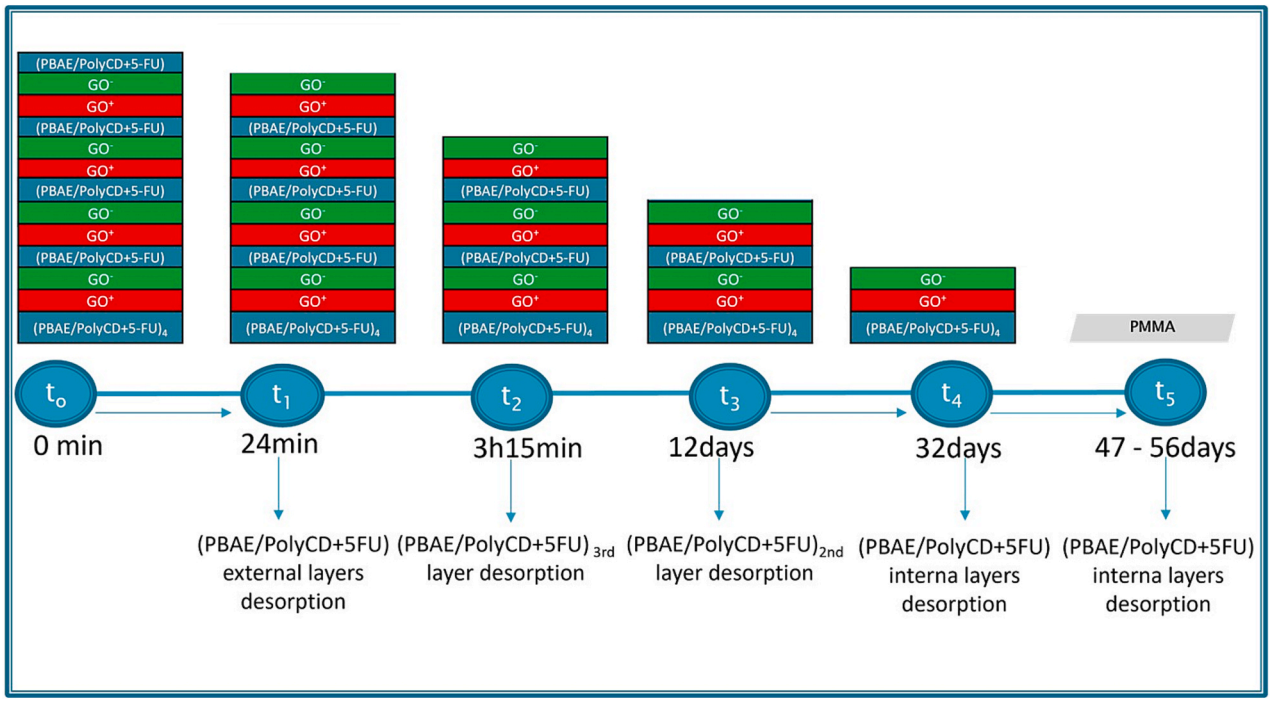

Fig. 11. Diagram of the time release of each drug delivery layer in a PMMA substrate. The external drug layer was released after 24 min, and all the drug delivery layers were released after 56 days.

defined plateaus corresponding to the film surface and the bare substrate, separated by a sharp step characteristic of the LBL coating. After baseline correction and removal of minor surface noise, the height difference between the plateaus was calculated by averaging multiple points within each region.

This analysis yielded an average film thickness of 16.2 nm (Fig. 15), confirming the successful deposition of a uniform eight-bilayer structure. The consistency of replicated measurements further indicates the reproducibility of the LBL assembly process and the mechanical stability of the deposited nanostructured film.

3.4. Quantification of 5-FU in the drug-delivery film

The amount of 5-FU incorporated into the LBL drug-delivery films was quantified using UV–Vis spectroscopy by comparing the drug concentration in solution before and after film fabrication. This indirect approach enabled determination of the mass of 5-FU incorporated into the multilayer structure.

UV–Vis absorbance spectra were recorded at 265.5 nm, corresponding to the characteristic absorption maximum of 5-FU. Quantification was performed using a previously established calibration curve obtained from standard 5-FU solutions prepared in sodium acetate buffer, ensuring consistent solvent conditions throughout the analysis.

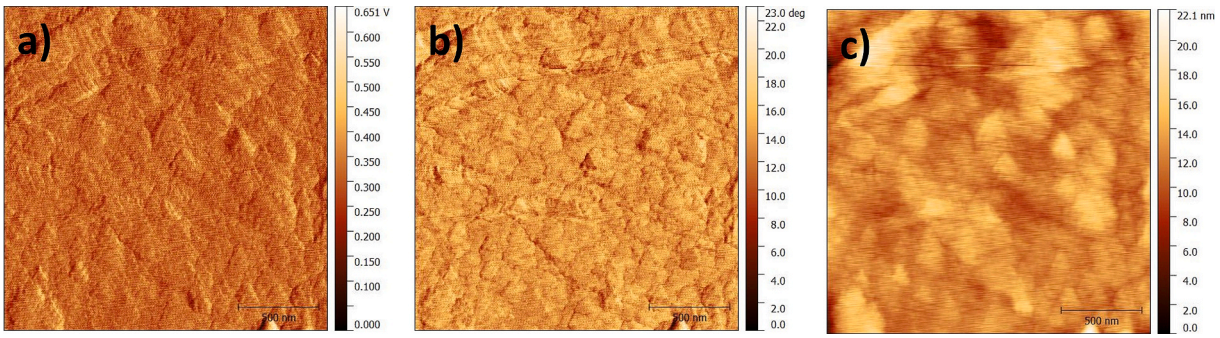

Fig. 12. (a) Amplitude, (b) phase and (c) topography AFM images from LBL assemblyPBAE/β-CD:5-FU/GO+/GO-/PBAE/ β-CD:5-FU − 2 μm, showing a smooth and continuous surface.

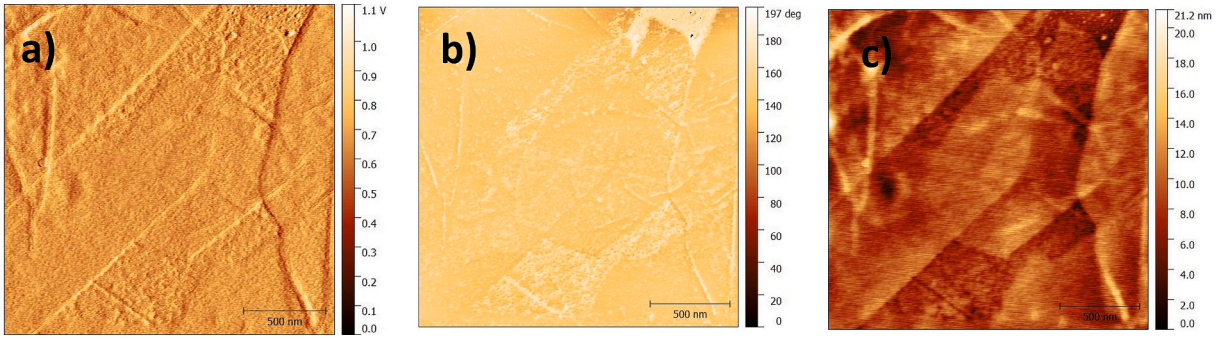

Fig. 13. (a) Amplitude, (b) phase and (c) topography AFM images from LBL assemblyPBAE/β-CD:5-FU/GO+/GO- −2 μm, showing rigid graphene domains.

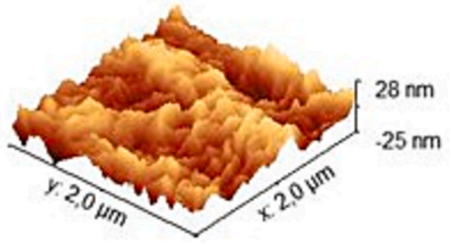

Fig. 14. AFM topography 3D image of β-CD:5-FU layer, showing a granular morphology characterized by densely packed features with height variations range approximately from −25 nm to 28 nm, indicating a moderate surface roughness at the nanoscale.

The reduction in absorbance observed after the film preparation was attributed to the incorporation of 5-FU into the LBL film.

Based on the calibration curve, the amount of 5-FU incorporated into the film was calculated to be 0.0189 mg. Considering an initial drug concentration of 0.0391 mg/ml, the drug load efficiency was approximately 48.3%, indicating that nearly half of the available 5-FU was successfully incorporated into the multilayer film.

To enable comparison with clinically relevant antimetabolite doses and account for film geometry, the amount of 5-FU incorporated into the LBL films was normalized to the film surface area. For a film area of 4.8 cm^2, the mass-normalized loading was calculated to be 3.94 μg/cm^2. In clinical glaucoma surgery, particularly following the implantation of glaucoma drainage devices, 5-FU is commonly administered through the application of surgical sponges soaked in concentrated drug solutions (typically 25.50 mg/ml) placed in contact with the subconjunctival tissues for several minutes in order to inhibit postoperative fibroblast proliferation and reduce fibrotic encapsulation around the implant (Lama and Fechtner, 2003; Khaw et al., 2001). Compared with these relatively high transient exposure concentrations, the drug loading achieved in the present LBL films is substantially lower; however, the multilayer architecture enables localized and sustained drug release at the implant interface. Importantly, prolonged exposure to low concentrations of 5-FU has been shown to effectively suppress fibroblast activity while reducing the adverse effects associated with high-dose bolus administration, including epithelial toxicity, wound leakage, hypotony and tissue necrosis (Greenfield et al., 1998; Wilkins et al., 2001). Therefore, the controlled release profile provided by the LBL films may maintain therapeutically relevant local concentrations over expended periods without reaching acutely toxic levels in surrounding ocular tissues. This sustained low-dose strategy is particularly advantageous in glaucoma drainage device surgery, where long-term modulation of wound healing is critical for preventing fibrotic capsule formation and maintaining aqueous humor drainage. Furthermore, the surface-normalized drug loading obtained in this study falls within a range considered suitable for localized antifibrotic activity while potentially improving tissue compatibility compared to conventional sponge-based delivery approaches.

3.5. *Literature data*

The biological relevance of the developed multilayer drug delivery system is closely associated with the well-established antifibrotic activity of 5-FU in glaucoma surgery. Excessive fibroblast proliferation and extracellular matrix deposition are recognized as the main causes of postoperative fibrosis and fibrotic capsule formation around glaucoma drainage devices, ultimately compromising aqueous humor drainage and long-term surgical success. *In vitro* studies have demonstrated that sustained exposure to relatively low concentrations of 5-FU is sufficient to inhibit fibroblast proliferation, migration, and collagen synthesis, all of which are critical processes involved in wound healing and scar formation following glaucoma surgery (Khaw et al., 2001; Mietz and Addicks, 1996).

Conventional clinical administration of 5-FU is generally achieved

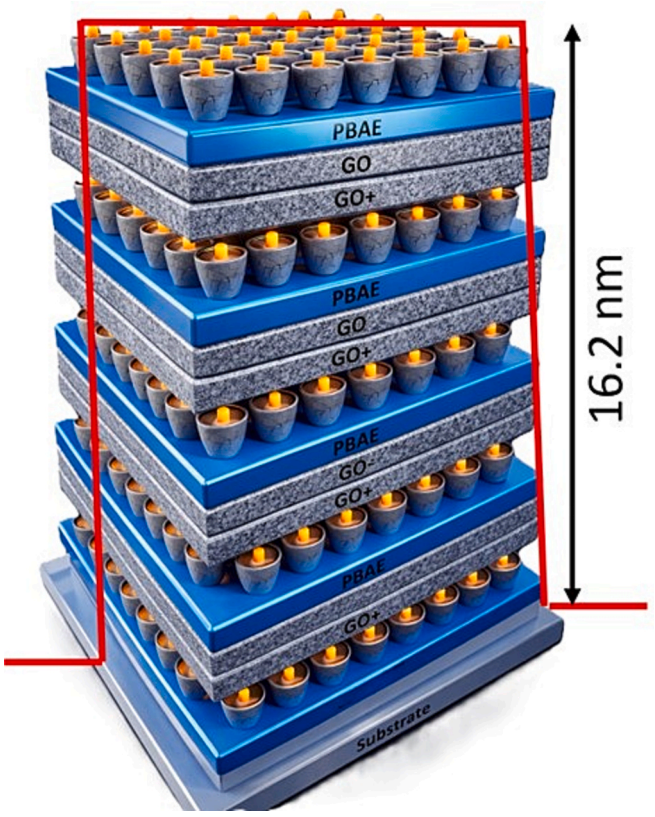

Fig. 15. Representative height profile obtained by stylus profilometry across a mechanical generated scratch on the 8-bilayer LBL film. The two plateau regions correspond to the coated surface and the exposed substrate, respectively. The step height between plateaus yields an average film thickness of 16.2 nm, confirming uniform film growth and successful multilayer assembly.

through intraoperative sponge application or repeated postoperative subconjunctival injections using highly concentrated solutions, typically ranging from 25 to 50 mg/ml (Lama and Fechtner, 2003). Although these approaches effectively reduce fibrosis, they are associated with several complications, including corneal epithelial toxicity, wound leakage, hypotony, bleb avascularity, and an increased risk of infection, largely due to high local drug exposure and the absence of controlled release (Khaw et al., 2001; Greenfield et al., 1998). Consequently, there has been considerable interest in developing localized sustained-delivery systems capable of maintaining therapeutic antifibrotic activity while minimizing tissue toxicity.

In this context, the LBL films developed in the present work were designed to provide controlled and prolonged release of 5-FU directly at the implant interface. Although the drug loading determined for the films (3.94 μg/cm^2) is substantially lower than the concentrations employed in conventional sponge-based administration, prolonged localized exposure to lower drug concentrations may still effectively modulate fibroblast activity. Previous studies have shown that continuous low-dose exposure to 5-FU can significantly inhibit fibroblast proliferation and activity while reducing cytotoxic side effects associated with bolus administration (Aref, 2017). Therefore, the sustained release profile observed for the multilayered films may help maintain biologically active concentrations within the *peri*-implant microenvironment over extended periods, which is particularly advantageous during the critical postoperative wound healing phase.

Additionally, the multilayer architecture based on alternating graphene oxide layers and cyclodextrin-containing reservoirs may further enhance therapeutic performance by limiting burst release and promoting gradual drug diffusion. Such behavior is highly desirable in glaucoma drainage device applications, where excessive early drug release may induce tissue toxicity, whereas insufficient long-term release may fail to prevent fibrotic encapsulation. The use of nanostructured LBL coatings therefore represents a promising strategy to achieve a balance between antifibrotic efficacy and tissue compatibility.

Furthermore, previous studies involving PBAE-based multilayer systems and graphene oxide-containing coatings have demonstrated favorable biocompatibility and suitability for biomedical and drug delivery applications. In addition, related multilayer architectures previously developed by our group for the controlled release of Brimonidine, a clinically established antiglaucoma drug, showed promising stability and compatibility for ophthalmic applications (Machado et al., 2019). These previous findings further support the rationale for employing the present multilayer platform in localized ocular drug delivery systems.

Despite these promising characteristics, it is important to acknowledge that the present study did not include direct biological evaluation of cytotoxicity, fibroblast proliferation, or antifibrotic efficacy. Consequently, the biological performance of the released 5-FU was inferred based on previously reported literature and the established pharmacological activity of the drug. Future studies should therefore include in vitro assays using ocular fibroblasts to assess cell viability, proliferation, extracellular matrix production, and inflammatory responses following exposure to the released drug concentrations. In addition, in vivo evaluation will be essential to determine the long-term therapeutic efficacy and safety of the developed coatings under physiologically relevant conditions.

The long-term release experiments performed in the present study were conducted under simulated physiological conditions using PBS (pH 7.4) at 37°C. Under these conditions, 5-FU is generally reported to exhibit relatively good aqueous stability, particularly in neutral and slightly acidic environments. Previous studies have demonstrated that 5-FU remains chemically stable in buffered aqueous solutions at physiological pH for extended periods, with degradation occurring mainly under strongly alkaline conditions, elevated temperatures, or prolonged light exposure (Diasio and Harris, 1989; Longley et al., 2003). This relative stability supports the assumption that the released drug largely preserves its chemical integrity during the experiments performed in this work.

Additionally, the incorporation of 5-FU within β-CD-containing multilayer architecture may further contribute to drug stabilization. Cyclodextrins are known to improve the physicochemical stability of encapsulated compounds by partially shielding them from hydrolytic and environmental degradation through host–guest interactions within their hydrophobic cavity (Loftsson and Duchêne, 2007). Therefore, the encapsulation strategy employed in the present system may provide an additional protective effect during prolonged exposure to aqueous physiological media.

Nevertheless, it is important to acknowledge that the chemical integrity of the released 5-FU was not directly evaluated by chromatographic techniques such as HPLC or liquid chromatography-mass spectrometry (LC-MS). Drug quantification in the present study was performed based on the characteristic spectroscopy response of 5-FU, assuming preservation of its molecular structure throughout the release period. Although the available literature supports the expected stability of 5-FU under the experimental conditions employed, the absence of direct analytical confirmation represents a limitation of this study.

Future work should therefore include chromatographic characterization of the released fractions to confirm the molecular integrity and pharmacological activity of 5-FU following prolonged release from the multilayer films. Such analyses will be particularly important for validating the long-term therapeutic performance of the developed platform and for excluding the presence of potential degradation products that may affect biological activity or tissue compatibility.

4. Discussion

The nanostructured films developed in this study were fabricated using a LBL approach, with the adsorption of each layer monitored by UV–Vis spectroscopy. For both quartz and PMMA substrates (Figs. 3 and 8), a progressive linear increase in absorbance intensity was observed with successive deposition cycles, confirming the sequential, uniform, and reproducible assembly of the multilayer architecture. This behavior is characteristic of well-controlled LBL systems and is consistent with previous studies demonstrating linear film growth driven by electrostatic interactions and stable multilayer deposition (Machado et al., 2019; Machado et al., 2025; Borges and Mano, 2015). The reproducibility observed in the present work therefore confirms the effective incorporation of both drug-delivery layers (β-CD:5-FU) and barrier-forming components (PBAE and GO), supporting the structural predictability required for programmable drug release.

A central finding of this work is the strong influence of both outer-layer composition and substrate properties on drug release kinetics. It is important to note that the multilayer architectures deposited on quartz and PMMA substrates were intentionally designed with distinct structural organizations in order to investigate different release strategies and evaluate the combined influence of substrate physicochemical properties and barrier layer composition on drug delivery behavior. Therefore, the comparison between both systems was not intended as a direct bilayer-to-bilayer equivalence, but rather as an assessment of how substrate-dependent film organization and multilayer architecture affect release kinetics under different structural configurations. In quartz-based films (Figs. 5–7), the release profile exhibited a stepwise behavior, where each increment in cumulative 5-FU release corresponded to the desorption of individual drug-loaded layers. The delayed release of the outermost layer (~12h42min) suggests the presence of a diffusion-limiting effect associated with the GO^{+}/GO^{-} barrier architecture. Similar delayed release behavior has previously been reported in graphene oxide-containing multilayer systems, where graphene nanosheets acted as dense nanobarriers capable of restricting solvent penetration and reducing molecular diffusion rates (Shim et al., 2008; Depan et al., 2011). The progressively increasing release times observed for deeper layers, extending up to ~94h42min, further suggest enhanced intermolecular interactions within the multilayer assembly. This behavior may be associated with stronger host–guest interactions between β-CD and 5-FU, as well as increasing diffusion resistance imposed by the multilayer architecture. Comparable sustained release profiles have been described in cyclodextrin-based thin films, where the inclusion complex stability contributed to prolonged drug retention and reduced burst release (Thatiparti and Von Recum, 2010).

In contrast, PMMA-based films exhibit a markedly different release mechanism, characterized by dual-phase behavior (Figs. 9–11). The rapid release of the outermost β-CD:5-FU layer within approximately 24 min is attributed to its direct exposure to the aqueous medium and the absence of a graphene-based barrier. Similar burst release phenomena have been extensively reported in multilayer systems lacking external diffusion-limiting coatings, particularly when hydrophilic surfaces facilitate rapid solvent uptake and polymer swelling (Wood et al., 2006). This initial burst was followed by a prolonged sustained release phase, extending up to 56 days, indicating the potential of the multilayer architecture to support long-term drug delivery. Sustained release over several weeks has similarly been observed in polymeric multilayer coatings incorporating biodegradable or diffusion-controlled barrier layers for ophthalmic and implantable drug delivery applications (Lee et al., 2010; Richardson et al., 2015). The release events occurring over approximately 32 days, followed by prolonged delivery from underlying "pillow" layers composed of PBAE/ β-CD:5-FU, suggest that the internal multilayer organization contributes to modulation of diffusion kinetics over extended periods.

The differences observed between quartz and PMMA substrates further highlight the critical role of substrate-dependent film dynamics. PMMA substrates likely promote increased hydration and polymer chain mobility due to their physicochemical properties, facilitating controlled diffusion through the multilayer structure. In contrast, quartz behaves as a rigid and relatively inert substrate, emphasizing barrier-controlled release mechanisms. Similar substrate-dependent effects on LBL film permeability and drug release kinetics have previously been described, where substrate stiffness and surface energy influenced film hydration, polymer rearrangement, and interfacial diffusion processes (Hammond, 2010).

Profilometry measurements confirmed the formation of a uniform eight-bilayer film with an average thickness of 16.2 nm (Fig. 15), indicating consistent layer growth and excluding thickness variability as a dominant factor influencing release behavior. Comparable nanoscale thicknesses have been reported for highly compact graphene oxide multilayers fabricated by LBL deposition, where film architecture rather than absolute thickness predominantly governed release kinetics (Kim et al., 2011). UV–Vis quantification further demonstrated that 0.0189 mg of 5-FU was incorporated into the multilayer structure, corresponding to a loading efficiency of 48.3% and a surface-normalized loading of 3.94 $\mu g cm^{-2}$. Although lower than the concentrations conventionally applied during glaucoma surgery through sponge administration, this loading falls within the range reported for sustained ophthalmic delivery systems designed to minimize toxicity while maintaining localized antifibrotic activity (Aref, 2017).

AFM analysis provided additional insight into the nanoscale mechanisms governing release behavior. The β-CD:5-FU outer layers exhibit smooth and homogeneous morphologies with low surface roughness and uniform phase contrast (Figs. 12 and 14), which may facilitate solvent diffusion and contribute to the sustained release behavior observed experimentally. Similar morphologies have been associated with improved drug diffusion and homogeneous release in polymeric LBL systems (Borges and Mano, 2015). Conversely, graphene-containing layers displayed increased roughness, sharp phase transitions, and heterogeneous rigid domains (Fig. 13), consistent with the formation of mechanically heterogeneous domains that may contribute to diffusion restriction. Previous studies have similarly demonstrated that graphene oxide incorporation increases film rigidity, decreases permeability, and creates tortuous diffusion pathways that delay molecular transport (Depan et al., 2011; Compton and Nguyen, 2010).

From a clinical perspective, the dual release behavior observed in PMMA-based systems may provide important therapeutic advantages for glaucoma drainage device applications. The initial burst release may contribute to the early modulation of postoperative fibroblast activity immediately following implantation, thereby reducing early-stage fibrosis. Subsequently, the prolonged sustained release phase may help maintain antifibrotic activity throughout the critical wound-healing period, minimizing delayed fibrotic encapsulation and preserving aqueous humor drainage. Sustained low-dose delivery strategies have previously been proposed as an effective alternative to repeated postoperative 5-FU injections, which are associated with epithelial toxicity and poor patient compliance (Lama and Fechtner, 2003; Aref, 2017). However, these potential therapeutic effects are inferred from previously reported biological responses to 5-FU and were not directly evaluated experimentally in the present study.

Overall, the present findings demonstrate that drug release kinetics in LBL films are governed by a synergistic interplay between multilayer composition, substrate properties, and nanoscale architecture. The incorporation of graphene-based barrier layers introduces controlled structural heterogeneity and diffusional resistance, allowing modulation of therapeutic release profiles. These results are in strong agreement with previous reports describing graphene oxide-based multilayers as versatile platforms for tunable and long-term drug delivery applications (Depan et al., 2011; Richardson et al., 2015).

Consequently, the developed multilayer coatings represent a promising strategy for advanced ophthalmic implants and localized glaucoma therapy.

Nevertheless, although the present study demonstrates the strong influence of multilayer architecture on drug release kinetics, future work should include fully standardized bilayer configurations across different substrates in order to enable more direct quantitative comparison of substrate-dependent release mechanisms under identical deposition conditions.

5. Conclusions

Effective modulation of postoperative wound healing remains a critical factor for the long-term success of glaucoma drainage surgeries. In particular, the ability to suppress excessive fibroblast proliferation while preserving normal tissue regeneration is essential to prevent device failure caused by fibrotic obstruction.

In the present study, a nanostructured multilayer film with time-controlled drug delivery capability was successfully developed for the sustained release of the antimitotic agent 5-FU. The encapsulation of 5-FU within β-CD improved its aqueous solubility and contributed to a more controlled release profile, potentially mitigating cytotoxic effects. The LBL assembly on both quartz and PMMA substrates exhibited linear and reproducible growth, confirming the ordered and reliable incorporation of drug-delivery and barrier components.

Comparative release studies demonstrated that graphene oxide (GO) layers play a key role in regulating drug release kinetics by acting as effective mass transport barriers. In quartz-based systems, GO enabled a stepwise and temporally resolved release, whereas in PMMA-based systems a biphasic release profile was observed, combining an initial burst release with prolonged sustained delivery. Notably, PMMA-supported films achieved complete drug release over approximately 56 days, closely matching the clinically relevant timeframe of post-operative wound healing.

The fabricated multilayer films exhibited high structural uniformity, with an average thickness of 16.2 nm and a drug loading efficiency of 48.3%, ensuring consistent and predictable drug availability at the target interface. Importantly, the PMMA substrate promoted a more sustained release profile compared to quartz, highlighting the advantages of polymeric materials commonly used in biomedical devices. The enhanced compatibility of PMMA with hydrated multilayer architectures supports stable diffusion pathways over extended periods, making it particularly suitable for postoperative environments. From a translational perspective, the combination of biocompatibility, optical transparency, flexibility, and tunable drug release, positions PMMA-based multilayer coatings as a promising platform for integration into glaucoma drainage devices.

Overall, this study demonstrates that the synergistic control of multilayer composition, nanoscale architecture, and substrate properties enables the design of advanced drug delivery systems with programmable release profiles. Such systems hold significant potential for improving both short and long-term surgical outcomes in glaucoma and other fibrosis-related conditions.

Declaration of generative AI and AI-assisted technologies in the writing process

During the preparation of this work the author(s) used ChatGPT in order to optimize the images. After using this tool/service, the author(s) reviewed and edited the content as needed and take(s) full responsibility for the content of the published article.

CRediT authorship contribution statement

Mónica Machado: Writing – original draft, Methodology, Investigation, Formal analysis, Conceptualization. **Gabriela Araujo Silva:** Validation, Writing – review & editing. **Joana Ferreira:** Writing – review & editing, Visualization. **Luis A. Pinto:** Writing – review & editing, Visualization. **Quirina Ferreira:** Writing – review & editing, Supervision, Investigation, Funding acquisition, Formal analysis.

Funding

This research was funded by Fundação para a Ciência e Tecnologia (FCT) through the projects iNOVA4Health, Translational Medicine program—UIDB/Multi/04462/2020; UIDB/50008/2020 and PTDC/CTM-REF/2679/2020.

Declaration of competing interest

The authors declare that they have no known competing financial interests or personal relationships that could have appeared to influence the work reported in this paper.

Acknowledgements

All authors acknowledge the iNOVA4Health—Translational Medicine program—UIDB/Multi/04462/2020, UIDB/50008/2020, and the SmartGlauco project—PTDC/CTMREF/2679/2020, which are both financially supported by Fundação para a Ciência e Tecnologia (FCT).

Data availability

Data will be made available on request.

References

Allison, K., Patel, D., Alabi, O., 2024. Epidemiology of glaucoma: the past, present, and predictions for the future. Cureus 12 (11), e11686. https://doi.org/10.7759/cureus.11686.

Aref, A.A., 2017. Sustained drug delivery for glaucoma. Curr. Opin. Ophthalmol. 28 (2), 169–174. https://doi.org/10.1097/ICU.0000000000000334.

Borges, J., Mano, J.F., 2015. Molecular interactions driving the layer-by-layer assembly of multilayers. Chem. Rev. 114 (18), 8883–8946. https://doi.org/10.1021/cr400531v.

Boyd, D., Young, A.M., Walker, G.S., et al., 1998. Biocompatibility of intraocular lens materials: randomized clinical trial. L Cataract Refract Surg. 24 (6), 857–862. https://doi.org/10.1016/S0886-3350(98)80180-1.

Choi, J., Zhang, C., Reipa, V., et al., 2014. Optical and biocompatibility properties of MA POSS-PMA for intraocular lenses. RSC Adv. 4, 43148–43155. https://doi.org/10.1039/C4RA08060B.

Compton, O.C., Nguyen, S.T., 2010. Graphene oxide, highly reduced graphene oxide, and graphene: versatile building blocks for carbon-based materials. Small 6 (6), 711–723. https://doi.org/10.1002/smll.200901934.

Depan, D., Shah, J., Misra, R.D.K., 2011. Controlled release of drug from folate-decorated and graphene mediated drug delivery system: synthesis, loading efficiency, and drug release response. Mater. Sci. Eng. C 31 (7), 1305–1313. https://doi.org/10.1016/j.msec.2011.04.010.

Diasio, R.B., Harris, B.E., 1989. Clinical pharmacology of 5-fluorouracil. Clin. Pharmacokinet. 16 (4), 215–237. https://doi.org/10.2165/00003088-198916040-00002.

Ferreira, Q., Sousa, C., et al., 2019. Layer-by-layer films of PBAE and graphene oxide for drug release control. Colloids Surf. B Biointerfaces 183, 110422. https://doi.org/10.1016/j.colsurfb.2019.110422.

Greenfield, D.S., Liebmann, J.M., Jee, J., Ritch, R., 1998. Late-onset bleb leaks after glaucoma filtering surgery. Arch. Ophthalmol. 116 (4), 443–447. https://doi.org/10.1001/archopht.116.4.443.

Guimarães, E.V.M., De Pádua Soares Bezerra, B., De Miranda Cordeiro, F., Carvalho, H.S. C., Daniff, N.D., Prata, S.T., Dorairaj, K.S., Kanadani, N.F., 2019. Glaucoma surgery with soaked sponges with Mitomycin C vs sub-tenon injection: short-term outcomes. J. Curr. Glaucoma Pract. 13 (2), 50–54. https://doi.org/10.5005/jp-journals-10078-1254.

Hammond, P.T., 2010. Building biomedical materials layer-by-layer. Mater. Today 15 (5), 196–206. https://doi.org/10.1016/S1369-7021(12)70090-1.

Hwang, H., Joo, P., Sung Kang, M., Ahn, G., Tark Han, J., Kim, B.-S., Ho Cho, J., 2012. Highly tunable charge transport in layer-by-layer assembled graphene transistors. ACS Nano 6 (3), 2432–2440. https://doi.org/10.1021/nn2047197.

Jampel, D., Henry, M.D., 1992. Effect of brief exposure to Mitomycin C on viability and proliferation of cultured human Tenon's capsule fibroblasts. Ophthalmology 99 (9), 1471–1476. https://doi.org/10.1016/s0161-6420(92)31781-6.

Júnior, E.R.S., Belfort, A.F.L., Pereira, V.C., 2025. Global and national epidemiology of glaucoma: prevalence, burden, and public health implications. Rev. Bras. Oftalmol. 84, e0094. https://doi.org/10.37039/1982.8551.20250094.

Kaliramna, S., Singh Dhayal, S., Kumar, N., 2022. Fabrication of PMMA thin film and its optical and photocatalytic activity. Mater. Today Proc. 69 (1), 42–46. https://doi.org/10.1016/j.matpr.2022.08.327.

Khaw, P.T., Doyle, J.W., Sherwood, M.B., et al., 2001. Advances in glaucoma surgery: evolution of antimetabolite adjunctive therapy. J. Glaucoma 10 (5), S81–S84. https://doi.org/10.1097/0061198-200110001-00029.

Kim, S., Ku, S.H., Lim, S.Y., et al., 2011. Graphene-biomineral hybrid materials. Adv. Mater. 23 (17), 2009–2014. https://doi.org/10.1002/adma.201100010.

Lama, P.J., Fechtner, R.D., 2003. Antifibrotics and wound healing in glaucoma surgery. Surv. Ophthalmol. 48 (3), 314–346. https://doi.org/10.1016/s0039-6257(03)00038-9.

Le Floch, F., Belbekhouche, S., Oniszczuk, J., Carbonnier, B., 2020. Smart polyelectrolyte multilayer coatings for drug delivery. Smart Nanocontainers 18, 295–314. https://doi.org/10.1016/B978-0-12-816770-0.00018-6.

Lee, S.S., Hughes, P., Ross, A.D., Robinson, M.R., 2010. Biodegradable implants for sustained drug release in the eye. Pharm. Res. 27 (10), 2043–2053. https://doi.org/10.1007/s11095-010-0159-x.

Loftsson, T., Duchêne, D., 2007. Cyclodextrins and their pharmaceutical applications. Int. J. Pharm. 329 (1–2), 1–11. https://doi.org/10.1016/j.ijpharm.2006.10.044.

Longley, D.B., Harkin, D.P., Johnston, P.G., 2003. 5-fluorouracil: mechanisms of action and clinical strategies. Nat. Rev. Cancer 3 (5), 330–338. https://doi.org/10.1038/nrc1074.

Luís Occhiutto, M., Maranhão, R.C., Paulino Costa, V., Konstas, G.A., 2019. Nanotechnology for medical and surgical glaucoma therapy – a review. Adv. Ther. 37, 155–199. https://doi.org/10.1007/s12325-019-01163-6.

Lynn, M.D., Langer, R., 2020. Degradable poly(β-amino esters): synthesis, characterization, and self-assembly with plasmid DNA. J. Am. Chem. Soc. 122, 10761–10768. https://doi.org/10.1021/ja00155388.

Machado, M., Silva, G.A., Bitoque, D.B., Ferreira, J., Pinto, L.A., Morgado, J., Ferreira, Q., 2019. Self-assembled multilayer films for time-controlled ocular drug delivery. ACS Appl. Bio Mater. 2 (10), 4173–4180. https://doi.org/10.1021/acsabm.9b00417.

Machado, M., Silva, G.A., Ferreira, J., Pinto, L.A., Ferreira, Q., 2025. Enhancement of the solubility of 5-fluorouracil through encapsulation within β-cyclodextrin to control fibroblast growth in glaucoma surgery. RSC Adv. 15, 33522–33530. https://doi.org/10.1039/d5ra03005f.

Mietz, H., Addicks, K., 1996. Histopathology of filtering blebs after long-term treatments with antimetabolites. Ophthalmic Surg. Lasers 27 (5), 379–384.

Peng, Y., Han, L., Jiang, Q., Liu, J., Liu, X., Jiang, G., Li, Z., Qin, S., Zhuo, Y., Su, W., 2026. Global, regional and national burden of glaucoma from 1990 to 2021 and projections to 2050: a retrospective cross-sectional study. BMJ Open 16 (1), e108975. https://doi.org/10.1136/bmjopen-2025-108975.

Rahic, O., Tucak, A., Omerovic, N., Sirbubalo, M., Hindija, L., Hadziabdic, J., Vranic, E., 2021. Novel drug delivery systems fighting glaucoma: formulation obstacles and solutions. Pharmaceutics 13 (28). https://doi.org/10.3390/pharmaceutics13010028.

Reinthal, K.E., Olivier Denk, P., Grub, M., Besch, D., Ulrich Bartz-Schmidt, K., 2007. Dose, timing and frequency of subconjunctival 5-fluorouracil injections after glaucoma filtering surgery. Graefe's Arch. Clin. Exp. Ophthalmol. 245, 369–375. https://doi.org/10.1007/s00417-006-0406-3.

Riaz, Y., Mehta, J.S., Wormald, R., et al., 2014. Comparing rigid PMMA and foldable intraocular lenses: a randomized controlled trial. Br. J. Ophthalmol. 98 (2), 246–251. https://doi.org/10.1136/bjophthalmol-2013-303938.

Richardson, J.J., Bjornmalm, M., Caruso, F., 2015. Technology-driven layer-by-layer assembly of nanofilms. Science 348 (6233). https://doi.org/10.1126/science.aaa2491.

Schoenberg, D.E., Blake, A.D., Beau Swann, F., Parlin, W.A., Zurakowski, D., Margo, E.C., Ponnusamy, T., John, T.V., Ayyala, S.R., 2015. Effect of two novel sustained-release drug delivery systems on bleb fibrosis: an in vivo glaucoma drainage device study in a rabbit model. Transl. Vis. Sci. Technol. 4 (3). https://doi.org/10.1167/tvst.4.3.4.

Shi, Z., Song, L., Zhang, T., 2019. Optical and electrical characterization of pure PMMA for terahertz wide-band metamaterial absorbers. J. Infrared Milimeter Terahertz Waves 40, 80–91. https://doi.org/10.1007/s10762-018-0553-8.

Shim, B.S., Podsiadlo, P., Kotov, N.A., 2008. Functionalized graphene sheets for polymer nanocomposites. Nat. Nanotechnol. 3 (6), 327–331. https://doi.org/10.1038/nnano2008.96.

Svetozarskiy, N.S., Andreev, N.A., Shvaikin, V.A., Scherbakova, V.S., Sporysheva, N.A., 2023. An easy and safe method of subconjunctival injection of antimetabolites in glaucoma surgery. Explor. Med. 4, 453–460. https://doi.org/10.37349/emed.2023.00155.

Thatiparti, T.R., Von Recum, H.A., 2010. Cyclodextrin complexation for affinity-based antibiotic delivery. Macromol. Biosci. 10 (1), 82–90. https://doi.org/10.1002/mabi.200900204.

Vision and Eye Research Institute, et al., 2024. Global estimates on the number of people blind or visually impaired by glaucoma: a meta-analysis from 2000 to 2020. Eye 38 (11), 2036–2046. https://doi.org/10.1038/s41433-024-02995-5.

Wei, Y., Chen, Y., Liu, P., Gao, Q., Sun, Yu., Huang, C., 2011. Surface modification of hydrophobic PMMA intraocular lens by the immobilization of hydroxyethyl methacrylate for improving application in ophthalmology. Plasma Chem. Plasma Process. 31, 811–825. https://doi.org/10.1007/s11090-0111-9323-2.

Wilkins, M., Indar, A., Wormald, R., 2001. Intra-operative Mitomycin C for glaucoma surgery. Cochrane Database Syst. Rev. 1, CD002897. https://doi.org/10.1002/14651858.CD002897.

Wood, K.D., Chuang, H.F., Batten, R.D., et al., 2006. Controlling interlayer diffusion to achieve sustained, multiagent delivery from layer-by-layer thin films. Proc. Natl. Acad. Sci. 103 (27), 10207–10212. https://doi.org/10.1073/pnas.0602884103.

Zhang, N., Wang, J., Li, Y., Jiang, B., 2021. Prevalence of primary open angle glaucoma in the last 20 years: a meta-analysis and systematic review. Sci. Rep. 11 (1), 13762. https://doi.org/10.1038/s41598-021-92971-w.